Jinst

Published by IOP Publishing for Sissa Medialab

Received: *February 10, 2020*
Revised: *April 2, 2020*
Accepted: *April 6, 2020*
Published: *May 15, 2020*

Investigation of nitrogen enriched silicon for particle detectors

J.C. Hönig,[a,1] **M. Baselga,**[b] **M. Centis Vignali,**[d] **L. Diehl,**[a] **A. Dierlamm,**[c] **E. Fretwurst,**[g] **P. Kaminski,**[e] **M. Moll,**[d] **F. Moos,**[a] **R. Mori,**[a] **U. Parzefall,**[a] **G. Pellegrini,**[f] **J.M. Rafí,**[f] **J. Schwandt**[g] **and L. Wiik-Fuchs**[a]

[a] *Physikalisches Institut, Albert-Ludwigs-Universität Freiburg, Hermann-Herder-Straße 3, 79104 Freiburg im Breisgau, Germany*
[b] *Deutsches Elektronen-Synchrotron, Notkestrasse 85, 22607 Hamburg, Germany*
[c] *Institute of Experimental Particle Physics, Karlsruhe Institute of Technology, Hermann-von-Helmholtz-Platz 1, D-76344 Eggenstein-Leopoldshafen, Germany*
[d] *EP Department, CERN, Esplanade des Particules 1, 1211 Geneva, Switzerland*
[e] *Łukasiewicz Research Network — Institute of Electronic Materials Technology, Wolczynska 133, 01-919 Warsaw, Poland*
[f] *Instituto de Microelectrónica de Barcelona, CNM-CSIC, Carrer dels Til·lers, Campus UAB, E-08193 Bellaterra, Spain*
[g] *Institute of Experimental Physics, University of Hamburg, Luruper Chaussee 149, D-22761 Hamburg, Germany*

E-mail: jan.hoenig@physik.uni-freiburg.de

Abstract: This article explores the viability of nitrogen enriched silicon for particle physics application. For that purpose silicon diodes and strip sensors were produced using high resistivity float zone silicon, diffusion oxygenated float zone silicon, nitrogen enriched float zone silicon and magnetic Czochralski silicon. The article features comparative studies using secondary ion mass spectrometry, electrical characterization, edge transient current technique, source and thermally stimulated current spectroscopy measurements on sensors that were irradiated up to a fluence of 10^{15} n_{eq}/cm^2. Irradiations were performed with 23 MeV protons at the facilities in Karlsruhe (KIT), with 24 GeV/c protons at CERN (PS-IRRAD) and neutrons at the research reactor in Ljubljana. Secondary ion mass spectrometry measurements give evidence for nitrogen loss after processing, which makes gaining from nitrogen enrichment difficult.

Keywords: Radiation-hard detectors; Solid state detectors

[1] Corresponding author.

https://doi.org/10.1088/1748-0221/15/05/P05006

2020 JINST 15 P05006

Contents

2020 JINST 15 P05006

1 Introduction

An approach to improve the radiation hardness of existing detector architectures is the use of float zone silicon which has been enriched with foreign atoms.

The ROSE collaboration used oxygen enriched float zone silicon to make existing detector architectures more resistant to changes in the effective doping concentration [1]. In oxygen enriched silicon the E(30K) defect is produced with a high rate under irradiation with hadrons [2]. This defect acts like a shallow donor making the material more n-type, which counteracts the usual change in effective doping concentration under irradiation that causes the material to become more p-type.

This effect is observed when the irradiation is being caused by charged particles. If irradiation is done with neutral particles, oxygenation does not provide any advantages.

A new candidate to enhance the performance of silicon in radiation environments is nitrogen [3]. The idea is that nitrogen interacts with vacancies during crystal growth and high temperature steps during detector fabrication. Vacancies are replaced with nitrogen (N_2) interstitials, which are more robust and localized than vacancies [4]. This paper presents the results of comparative performance studies between nitrogen enriched silicon detectors and detectors stemming from silicon wafers processed in different procedures. The study was designed to investigate possible advantages of nitrogen enrichment for silicon particle detectors.

2 Materials and methods

The study is based on n-type wafers with 300 µm thickness, which were produced in four different production procedures:

- Float zone (FZ)
- Float zone enriched with nitrogen (NIT)
- Float zone enriched with oxygen (DOFZ)
- Magnetic Czochralski (MCz)

The float zone wafers were produced at TopSil [5], the Magnetic Czochralski wafers at Okmetic [6]. Six wafers were processed into detectors from each of the four production procedures.

Device processing was carried out at the Institute of Microelectronics of Barcelona (IMB-CNM) cleanroom based on a well-established planar p-on-n fabrication process [7]. Wafer processing involved a 1100 °C processing step in wet ambient. The di-interstitial nitrogen defect is only stable up to 900 °C and thus the high temperature process at 1100 °C is a possible cause for nitrogen loss [8, 9]. Furthermore nitrogen increases oxygen precipitation in silicon after heat treatment [10].

In total 156 sensors and 120 diodes per type were produced, with a single wafer containing 26 strip sensors and 20 diodes. The strip sensors feature an active area of 1 cm × 1 cm and a pitch of 80 µm. The diodes have an active area of 4336 µm × 4336 µm.

2.1 Samples

To evaluate the sensors and diodes performance in environments with high radiation they were subject to an irradiation campaign. Irradiation was done at the following facilities:

- The Reactor Centre in Ljubljana with neutrons using a hardness factor of 0.9 [11].
- The Irradiation Center Karlsruhe with 23 MeV protons using a hardness factor of 2.0 [12].
- The PS-IRRAD Proton Facility at CERN with 24 GeV/c protons using a hardness factor of 0.62 [13].

Strip sensors were irradiated up to fluences of 1×10^{14} n_{eq}/cm^2, 3×10^{14} n_{eq}/cm^2, 6×10^{14} n_{eq}/cm^2 and 1×10^{15} n_{eq}/cm^2. Diodes were irradiated to the same fluences as well as 2×10^{11} n_{eq}/cm^2, 5×10^{12} n_{eq}/cm^2, 1×10^{13} n_{eq}/cm^2 and 5×10^{13} n_{eq}/cm^2. Two samples per type, fluence and irradiation facility, were prepared. The irradiated samples were subjected to an annealing study at 60 °C or 80 °C. The heat treatment was performed in an oven and annealing time is renormalized to the equivalent annealing at 21 °C room temperature using the parameters in [14].

2.2 Electrical characterization

After dicing electrical characterization was performed with a custom designed setup that allows for temperature control and a dry environment with relative humidity below 10 %. The capacitance-voltage characteristic (CV-curve) of the sensors and diodes was measured in the parallel mode (C_p-R_p) of the LCR meter. Frequency was set to 500 Hz and ramping was done in steps of 1 V, with a waiting time of 300 ms between voltage steps. Measurements were done in steps of 10 V with a settling time of 5 s.

2020 JINST 15 P05006

2.3 Beta source setup

Source measurements were performed in Karlsruhe and Freiburg. Both institutes conducted measurements at temperatures in the range of −14 °C to −30 °C and at a relative humidity of less than 10 %. The ALIBAVA readout system [15] was used, which is based on the Beetle ASIC. It provides separate channels to 128 of the 131 strips with a shaping time of about 25 ns [16]. Measurements are performed using a ^{90}Sr beta source. Depending on the site the measurements were performed at, the readout is triggered by a single scintillator (KIT) or two scintillators (Freiburg) in coincidence. In Freiburg only events falling into a time window of 10 ns around the signal peak are selected to allow for high statistics. The collected charge is determined using a clustering algorithm with a seed strip cut of 3.5 and a neighbouring cut of 1.8 times the noise value. In Karlsruhe −10 % around the signal peak are accepted which leads to a time window of roughly 25 ns. The seed cut is set to 4 and the neighbouring cut to 2 times the noise value.

2.4 Edge TCT

Laser measurements were conducted using the **T**ransient **C**urrent **T**echnique with a laser shining on the sensor edge (Edge TCT). The setup used is a standard `Particulars` Edge TCT setup [17, 18], featuring a fibre coupled laser with emitting a beam with a wavelength of 1064 nm. This laser is set to pulsed mode with a repetition rate of 5 kHz with 1 ns pulses. The setup is temperature controlled and stable to −32±0.5 °C with relative humidity below 20 %. The laser has a fixed focal point with a beam spot size below 11 µm, the position of that focal point can be changed by a motor stage [18]. A further description of the system is found in [19]. In charge collection measurements the laser beam moves in steps of 10 µm while the signal is sampled 300 times at each point.

2.5 TSC setup

The **T**hermally **S**timulated **C**urrent technique (TSC) is able to characterise radiation induced defects. The experimental setup consists of a closed cycle helium cryostat, which cools the samples down to a temperature around 10 K. From there defect levels are filled with charge carriers by applying a forward current in the order of 1 mA to the sensor. Thereafter the sensor is put in reverse bias and heated up with a constant and slow rate of 0.183 K s^{-1}. The analysis of the TSC spectra is performed using a single trap model and a fully depleted device. More details about the TSC technique and possible methods for the extraction of trap parameters can be found in [20–23].

3 Experimental results

3.1 SIMS measurements

To determine the exact nitrogen content Eurofins EAG Materials Science [24] measured the nitrogen content using a **S**econdary **I**on **M**ass **S**pectrometry setup (SIMS). The detection limit for nitrogen within their measurements was 1×10^{15} at/cm^3. The results are displayed in figure 1. Unprocessed wafers as received from Topsil showed a nitrogen content of 2.4×10^{15} at/cm^2. After wafer processing, the measured nitrogen content in this case was at or below the detection limit of 1×10^{15} at/cm^3.

2020 JINST 15 P05006

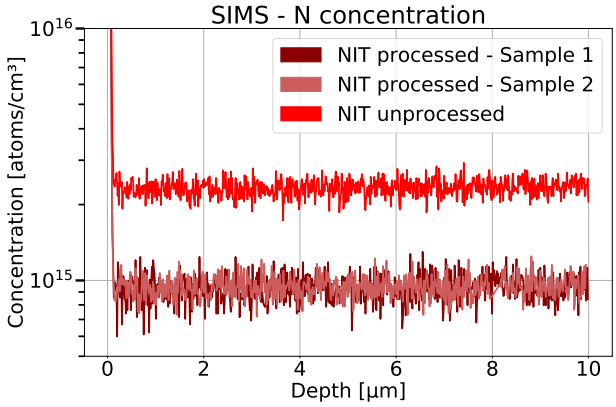

Figure 1. First measurement was conducted with raw wafer material. In a second stage a NIT sensor with the back metal layer removed and a NIT sensor with the back metal layer removed plus an unmasked back etch of silicon to a final sample thickness of about 137 µm were measured. The detection limit was at 10^{15} atoms/cm^3.

The most dominant form of nitrogen in silicon is the di-interstitial nitrogen defect [25]. This defect is very stable with the binding energy of the two nitrogen atoms being 3.67 eV and was expected to lead to increased radiation hardness [8]. However the di-interstitial nitrogen defect is only stable up to 900 °C and thus the high temperature processing is the most likely cause for the nitrogen loss [8, 9]. The thermal budget to which the wafers were exposed during device processing was dominated by the initial oxidation steps at 1100 °C, with a total estimated time of about 4 h. Thus possible improvements from nitrogen enrichment will be smaller than shown in [3]. The following measurements will aim to understand, if any advantages from nitrogen enrichment are retained.

3.2 Electrical characterization

In figure 2 the diode current-voltage characteristics of unirradiated sensors processed in the four different wafer types are displayed. Figure 3 shows the change in effective doping concentration as a function of the irradiation. The samples are named in the legend following the format *sample-type*-`irradiation-type` with *prot* meaning irradiation with 24 GeV/c protons and *neut* meaning irradiation with reactor neutrons. Looking at the change in effective doping concentration for the neutron irradiated samples, no large change in effective doping concentration is observed for the various float zone processed samples. For DOFZ this result is expected, as measurements done in [1] show that no improvements were observed for oxygenated silicon under irradiation with neutrons. For NIT the predicted improvements from measurements done in [3] could not be confirmed. The most likely cause being the lower concentration of the di-interstitial nitrogen defect. Nonetheless, effects could become visible once the device is annealed, as according to [26] nitrogen should make the silicon more resistant against dislocations. Which could also fix defects in place within the material. This is tested in source measurements in section 3.3.

Evaluating the proton irradiated samples in figure 3, again NIT shows similar depletion voltages as FZ. In contrast the DOFZ sample proved to be less susceptible towards changes in effective doping concentration, which was also observed in [1]. Finally the samples which proved most resistant to changes in effective doping concentration were the MCz samples, both under irradiation with neutrons as well as protons.

2020 JINST 15 P05006

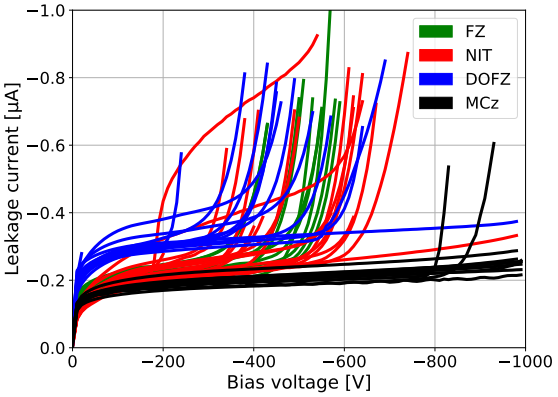

Figure 2. IV curves of unirradiated sensors from the test sample pool in Freiburg. Sensors were measured under laboratory conditions.

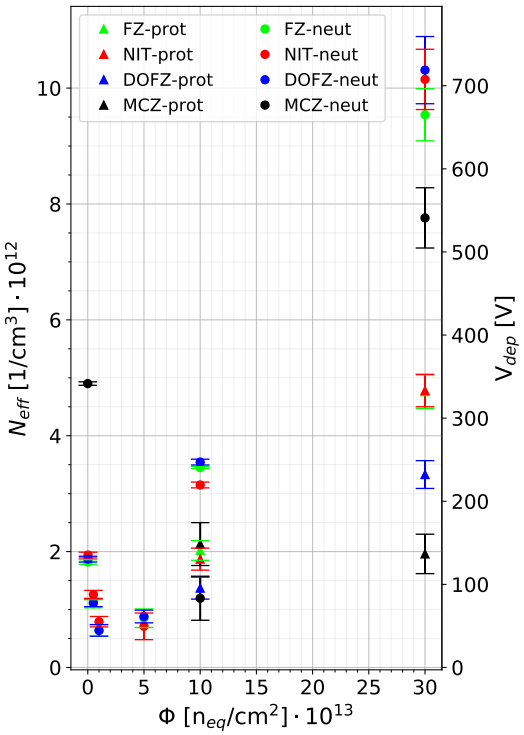

Figure 3. Effective doping concentration as a function of fluence. Low fluences between 5×10^{12} n_{eq}/cm^2 and 5×10^{13} n_{eq}/cm^2 were measured on diodes. Relative humidity below 10 % and temperature at −20 °C for sensors irradiated to 10^{14} n_{eq}/cm^2 or less and −25 °C for sensors irradiated to 3×10^{14} n_{eq}/cm^2.

3.3 Beta source measurements

Figure 4 shows the charge collection as a function of annealing time. The signal is normalized to electrons and the measurement was performed at a bias voltage of V_{bias} = 800 V. It was repeated for each sensor type at each of the four available fluences. Before irradiation the sensors from all wafers showed a charge collection between 23 000 e^- to 23 500 e^-. Until around 400 h of annealing at room temperature equivalent the sensors are still within beneficial annealing, where the 6×10^{14} n_{eq}/cm^2 NIT sensor showed higher charge collection than the other sensor types until 300 h [14]. Going beyond beneficial annealing the charge collection decreases in the reverse annealing phase and differences between the different detector types become apparent. Nonetheless, all sensor types show similar charge collection at lower fluences. The picture changes for fluences higher than 6×10^{14} n_{eq}/cm^2. Among the different float zone grown samples DOFZ shows the best performance with a charge collection around 8×10^3 e^- after 10 000 h annealing for the 1×10^{15} n_{eq}/cm^2 sample. The NIT and FZ sample show worse performance than the DOFZ sample and show roughly the same charge collection. Nonetheless, the NIT sample which was irradiated up to 1×10^{15} n_{eq}/cm^2 showed slightly higher charge collection for annealing times beyond 1000 h, but dropped strongly, barely collecting any charge, after 10 000 h.

2020 JINST 15 P05006

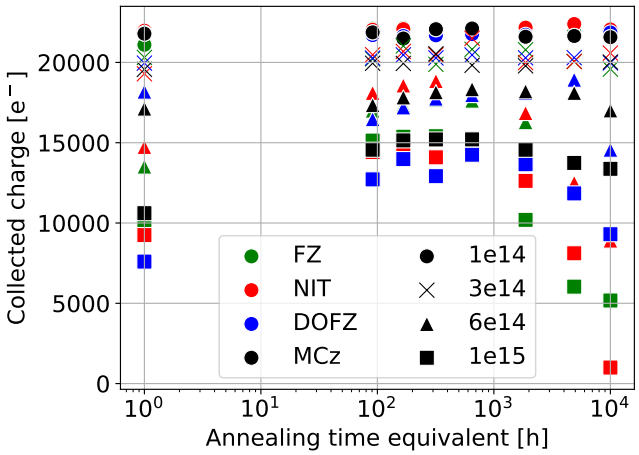

Figure 4. Charge collection as a function of annealing time at 800 V. The annealing was performed at 60 °C and renormalized to room temperature according to [14]. The measurements were performed at a temperature of −20 °C. Irradiation was performed with 23 MeV protons.

The neutron irradiated samples were measured on a different setup at a voltage of 700 V. Nevertheless the different float zone samples show roughly the same trend in charge collection with the only exception being DOFZ that shows the smallest charge collection which is consistent with [1]. The MCz samples showed high charge collection for all annealing times and fluences. Even at 1×10^{15} n_{eq}/cm^2 and 10 000 h annealing the MCz sample still showed charge collection around 1.4×10^3 e^-. In conclusion no NIT sample proved superior in charge collection over the full annealing period.

3.4 Edge TCT

The Edge TCT measurements were recorded with strip sensors. The collected charge plotted as a function of the laser position is displayed in figure 5. The charge generated at each position was measured for bias voltages spanning from 0 V to 300 V. In all graphs smaller depth corresponds to moving closer to the top of the sensor (p^+-strip side) while higher depth corresponds to moving closer to the bottom of the sensor (n^+ side). The six graphs in figure 5 show sensors which were irradiated to a fluence of 10^{14} n_{eq}/cm^2. The sensors irradiated to higher fluences show similar behaviour. The three top plots in figure 5 show sensors which were irradiated with reactor neutrons. If one interprets growing charge collection as the sensor depleting more and more with higher voltages, then all three sensors deplete from back to front. Which confirms that they are fully type inverted at this fluence. No large differences are visible between NIT and FZ after irradiation with neutrons.

Figure 5 on the bottom displays sensors which were irradiated with 24 GeV/c protons. The FZ sensor on the bottom right is type inverted depleting from back to front. In contrast the NIT sensor displayed in the bottom left in figure 5, seems not fully type inverted. It is depleting from front and back at lower voltages. The DOFZ sensor also depletes from front and back. To see the differences in field configuration more clearly it is necessary to look at the signals.

2020 JINST 15 P05006

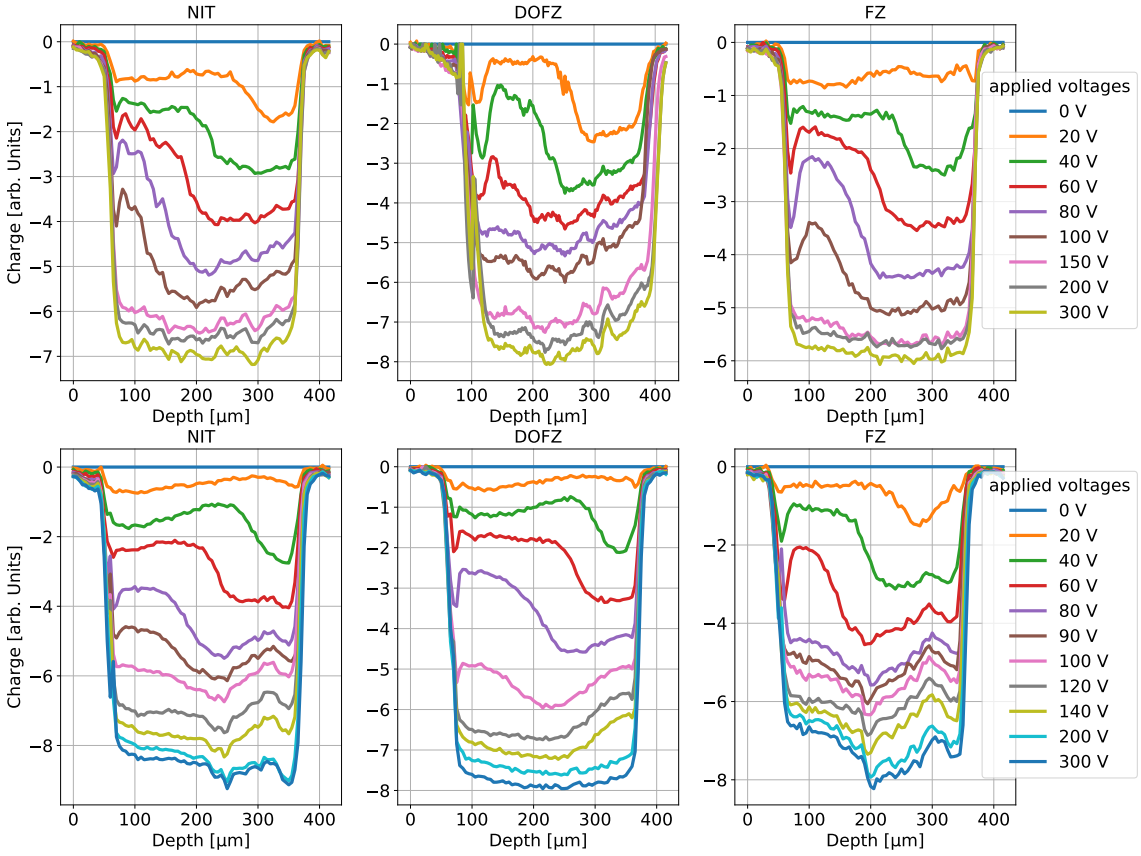

Figure 5. Charge collection of sensors irradiated to 10^{14} n_{eq}/cm^2. Sensors on the top were irradiated with reactor neutrons, sensors on the bottom with 24 GeV/c protons. The measurements were performed at a relative humidity below 20 % and temperature at −22 °C for the lower three plots and −20 °C for the upper three plots.

Figure 6 shows the response curves of the three proton irradiated sensors as a function of time. Each of the curves was recorded as the average of the detector response over 300 laser pulses at three different laser positions. Comparing the signals of the different sensor types it is possible to distinguish that the pulses for NIT and DOFZ at low voltages (40 V and 100 V) are longer than the pulses for FZ, close to the top and bottom of the sensors. The pulse shape is directly dependent on the field configuration within the sensor. Overall the signal plots show that the field configuration of the NIT sample is closer to the DOFZ sample than to the FZ sample. The similar behaviour of NIT and DOFZ could be a result of increased oxygen precipitation in the NIT sample [10]. Thus the NIT samples could contain slightly oxygen enriched regions after processing, influencing the results of the strip which is measured here.

Finally using the slope of the signal to calculate the electric field according to [27] confirms that DOFZ and NIT are depleting from both sides, while FZ is almost exclusively depleting back to front. In general more highly irradiated samples of any type showed a double-junction structure [28].

Overall in terms of field configuration no effect compared to FZ could be detected for NIT under irradiation with neutrons, while slight changes could be seen for NIT under irradiation with protons.

2020 JINST 15 P05006

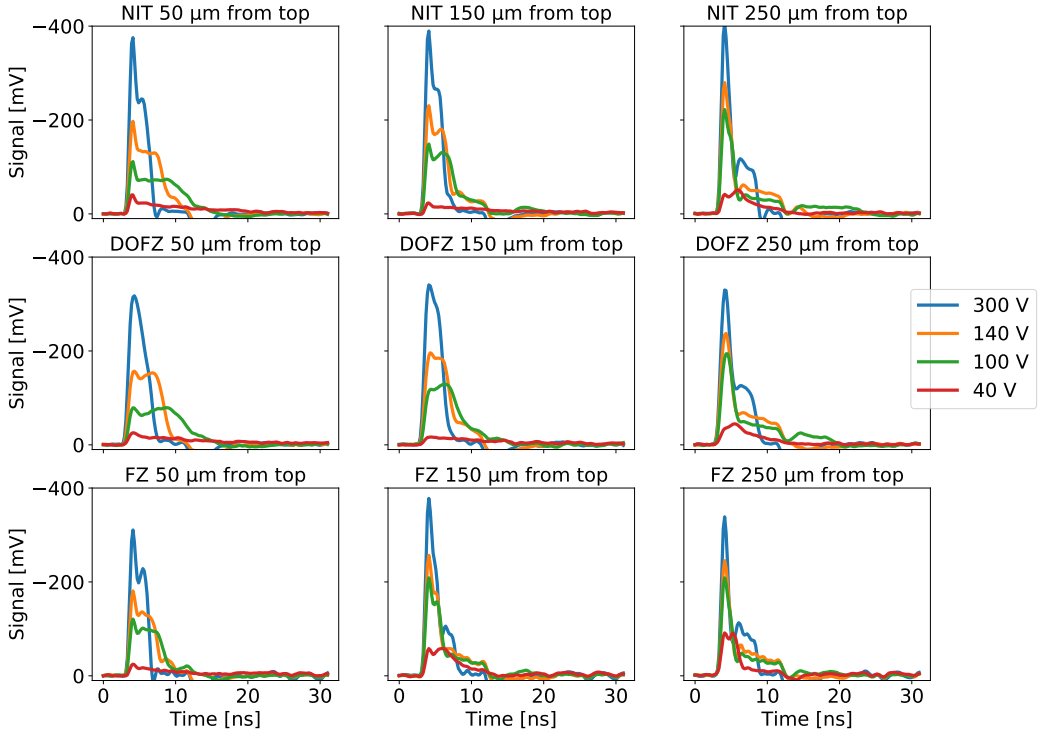

Figure 6. Amplified signal response from three sensors which were irradiated with 24 GeV/c protons to a fluence of 10^{14} n_{eq}/cm^2. Three laser positions are recorded, one close to the top, centre and bottom of the sensor. The measurements were performed at a relative humidity below 20 % and a temperature of −22 °C.

3.5 TSC measurements

The TSC measurements were recorded on diodes which were irradiated up to a fluence of 1×10^{13} n_{eq}/cm^2. Figures 7 and 8 show the resulting emission spectra. Only the most significant TSC peaks are labeled. TSC peaks labeled E and H are attributed to electron- and hole-traps, respectively. Figure 7 shows two samples (NIT and FZ) which were irradiated with neutrons and annealed at 60 °C for 80 min. The two spectra are nearly identical, except for the VO_i complex. This defect is more pronounced in NIT than in FZ, but the defect is not electrically active at room temperature and consequently not visible in tests of macroscopic properties [29]. Finally the broad peak at about 180 K is composed of at least five defect levels which are assumed to be higher order vacancy-related extended (clustered) defects ($E205_a$, V_2, V_3, H(220K), and I_p) [30, 31]. Nitrogen in silicon should lead to a distinct lower introduction of vacancy related agglomerates and decrease the concentration of this peak [4]. Overall this TSC measurement confirms the previous results which did not show improved results for nitrogen enriched material after irradiation with neutrons.

Figure 8 shows two samples which were irradiated with 24 GeV/c protons to a fluence of 1.4×10^{13} n_{eq}/cm^2. The E(30K), VO_i, $C_i^{(+/0)}$+H(116K) and H(140K)+H(152K) show different concentrations. The H(116K) is a deep acceptor in the lower half of the band which contributes with negative charge to the space charge. Consequently the lower concentration of H(116K) could be responsible for the differences in field configuration that were observed in the Edge TCT measurements (section 3.4). Furthermore the higher $C_i^{(+/0)}$+H(116K) signal for FZ could be caused

2020 JINST 15 P05006

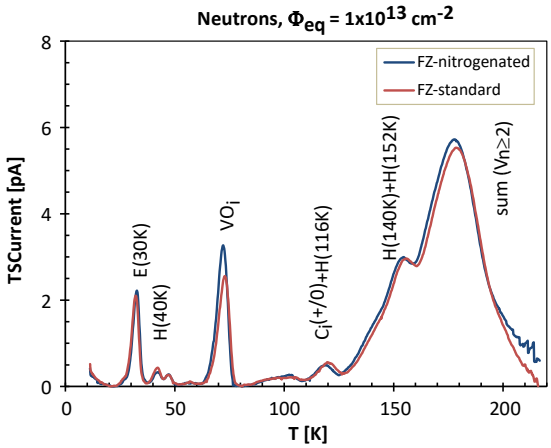

Figure 7. TSC spectra for NIT and FZ diodes irradiated with 1×10^{13} n_{eq}/cm^2 neutrons and after annealing for 80 min at 60 °C. Measurement details see section 2.5.

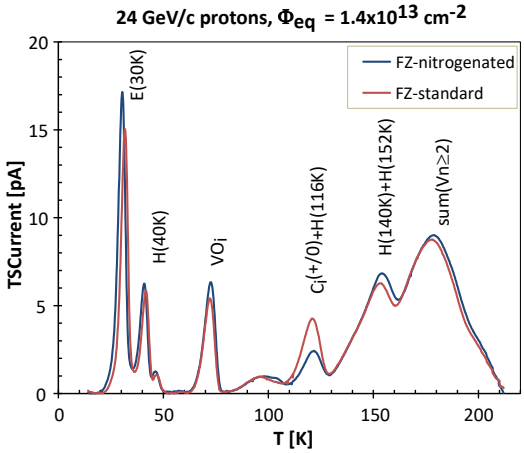

Figure 8. TSC spectra for NIT and FZ diodes irradiated with 1.4×10^{13} n_{eq}/cm^2 24 GeV/c protons and after annealing for 80 min at 60 °C. Measurement details see section 2.5.

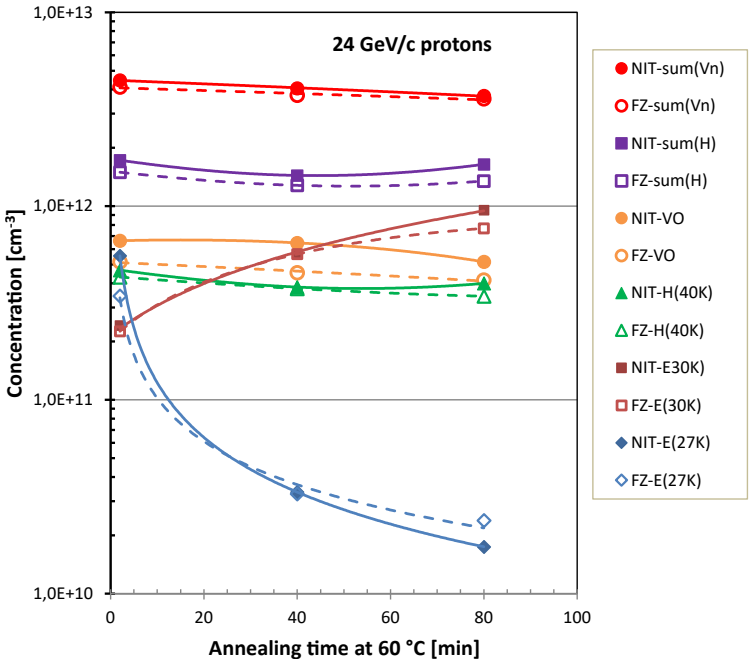

Figure 9. Development of defect concentration after irradiation with 24 GeV/c protons to 1.4×10^{13} n_{eq}/cm^2 as a function of annealing time at 60 °C. The filled symbols are attributed to NIT, the open symbols to FZ.

by a lower oxygen content and therefore a lower transformation rate to C_iO_i [14]. However one cannot extract the concentration of $C_i^{(+/0)}$ and $H(116K)$ separately. Thus larger annealing times are needed in order to come to a more quantitative conclusion about the concentration of $H(116K)$.

The emission of charge carriers from defects represented by the peaks shown in figure 8 have been fitted for different annealing times and the resulting concentrations are shown in figure 9 for both materials. The defect concentration is mainly constant for increasing annealing time and

2020 JINST 15 P05006

identical for FZ and NIT. Only the $E(30\text{K})$ defect increases and the defect $E(27\text{K})$ decreases with annealing time. The $E(27\text{K})$ is a possibly a precursor for the development of the $E(30\text{K})$ defect.

In summary, from these microscopic studies it is concluded that the difference in concentration of higher order vacancy related defects in NIT material compared to FZ is marginal. This is the case after neutron as well as high energy proton irradiation. The aforementioned similarity of NIT and FZ samples confirms an insignificant nitrogen content in the material, causing the expected reduction of the vacancy agglomerates to be undetectable.

4 Conclusion

Strip sensors and diodes based on silicon grown with different methods were investigated. The samples included float zone silicon, nitrogen as well as oxygen enriched float zone samples and Magnetic Czochralski silicon.

SIMS measurements showed that nitrogen is lost during sensor processing and the concentration is at least decreased down to the detection limit. Electrical characterization confirmed the expected behaviour of FZ and DOFZ. Hence no improvements in terms of effective doping concentration could be observed for NIT. Moreover, measurements with a beta source showed strongly decreasing performance at radiation doses beyond $6 \times 10^{14}\,\mathrm{n_{eq}/cm^2}$ for all float zone sensor types. Merely MCz proved resistant towards irradiation. Under investigation with an Edge TCT setup NIT and FZ neutron irradiated samples showed the same behaviour. Albeit the Edge TCT measurements done with proton irradiated samples showed NIT behaving more similar to DOFZ than FZ, with NIT being not fully type inverted at $1 \times 10^{14}\,\mathrm{n_{eq}/cm^2}$. A possible cause could be increased oxygen precipitation within the NIT sample.

Overall the remaining nitrogen concentration after processing seems to be too low to allow for improvements of particle detector characteristics.

Acknowledgments

This project has received funding from the European Union's Horizon 2020 Research and Innovation programme under Grant Agreement no. 654168.

This work has been partially financed by Spanish Ministry of Education and Science through project FPA2015-69260-C3-3-R (MINECO/FEDER UE) and it has made use of the Spanish ICTS Network MICRONANOFABS.

The nitrogen-lean and nitrogen-enriched FZ wafers used in this work were produced by Topsil Semiconductor Materials S.A. in Warsaw within the framework of the NitroSil project supported by the National Center for Research and Development under Grant Agreement No. PBS2/A9/26/2014.

We would like to give out special thanks to the CERN RD50 collaboration for their support and feedback during the course of our investigation.

2020 JINST 15 P05006

References

[1] ROSE collaboration, *Radiation hard silicon detectors — developments by the RD48 (ROSE) Collaboration*, *Nucl. Instrum. Meth.* **A 466** (2001) 308.

[2] M. Scaringella et al., *Localized energy levels generated in Magnetic Czochralski silicon by proton irradiation and their influence on the sign of space charge density*, *Nucl. Instrum. Meth.* **A 570** (2007) 322.

[3] P. Kamiński et al., *Effect of Nitrogen-Doping on the Properties of Radiation Defect Centers in FZ Silicon*, *SSP* **242** (2015) 279.

[4] W. von Ammon, R. Hölzl, J. Virbulis, E. Dornberger, R. Schmolke and D. Gräf, *The impact of nitrogen on the defect aggregation in silicon*, *J. Cryst. Growth* **226** (2001) 19.

[5] *Topsil*, http://www.topsil.com/.

[6] *Okmetic*, https://www.okmetic.com/.

[7] G. Pellegrini, J.M. Rafí, M. Ullán, M. Lozano, C. Fleta and F. Campabadal, *Characterization of magnetic Czochralski silicon radiation detectors*, *Nucl. Instrum. Meth.* **A 548** (2005) 355.

[8] N. Fujita, R. Jones, J.P. Goss, P.R. Briddon, T. Frauenheim and S. Öberg, *Diffusion of nitrogen in silicon*, *Appl. Phys. Lett.* **87** (2005) 021902.

[9] V.V. Voronkov and R. Falster, *Multispecies nitrogen diffusion in silicon*, *J. Appl. Phys.* **100** (2006) 083511.

[10] F. Shimura and R.S. Hockett, *Nitrogen effect on oxygen precipitation in Czochralski silicon*, *J. Appl. Phys.* **48** (1986) 224.

[11] *Reactor Centre in Ljubljana*, http://www.rcp.ijs.si/en/.

[12] *Irradiation Center Karlsruhe*, https://www.etp.kit.edu/english/irradiation_center.php.

[13] *PS-IRRAD Proton Facility*, http://ps-irrad.web.cern.ch/.

[14] M. Moll, *Radiation damage in silicon particle detectors: Microscopic defects and macroscopic properties*, Ph.D. Thesis, Hamburg U. (1999) [DESY-THESIS-1999-040].

[15] ALIBAVA collaboration, *A portable readout system for silicon microstrip sensors*, *Nucl. Instrum. Meth.* **A 623** (2010) 207.

[16] M. Agari et al., *Beetle — A radiation hard readout chip for the LHCb experiment*, *Nucl. Instrum. Meth.* **A 518** (2004) 468.

[17] G. Kramberger, *Advanced Transient Current Technique Systems*, PoS(Vertex2014)032 (2015).

[18] *Particulars*, http://www.particulars.si/products.php?prod=scanTCT.html.

[19] G. Kramberger et al., *Investigation of Irradiated Silicon Detectors by Edge-TCT*, *IEEE Trans. Nucl. Sci.* **57** (2010) 2294.

[20] M. Bruzzi, *TSC data-analysis on heavily irradiated silicon detectors*, *Nucl. Instrum. Meth.* **A 352** (1995) 618.

[21] M.G. Buehler, *Impurity centers in PN junctions determined from shifts in the thermally stimulated current and capacitance response with heating rate*, *Solid State Electron.* **15** (1972) 69.

[22] I. Pintilie, L. Pintilie, M. Moll, E. Fretwurst and G. Lindstroem, *Thermally stimulated current method applied on diodes with high concentration of deep trapping levels*, *Appl. Phys. Lett.* **78** (2001) 550.

2020 JINST 15 P05006

[23] H. Feick, E. Fretwurst, P. Heydarpoor, G. Lindström and M. Moll, *Analysis of TSC spectra measured on silicon pad detectors after exposure to fast neutrons*, *Nucl. Instrum. Meth.* **A 388** (1997) 323.

[24] *Eurofins EAG Materials Science*, https://www.eurofins.com/.

[25] R. Jones, S. Öberg, R.F. Berg and N.B. Bech, *Identification of the dominant nitrogen defect in silicon*, *Phys. Rev. Lett.* **72** (1994) 1882.

[26] K. Sumino, I. Yonenaga, M. Imai and T. Abe, *Effects of nitrogen on dislocation behavior and mechanical strength in silicon crystals*, *J. Appl. Phys.* **54** (1983) 5016.

[27] G. Kramberger, V. Cindro, I. Mandic, M. Mikuz, M. Milovanovic and M. Zavrtanik, *Investigation of electric field and charge multiplication in silicon detectors by Edge-TCT*, *IEEE Trans. Nucl. Sci.* (2009) 1740.

[28] E. Verbitskaya, V. Eremin, Z. Li, J. Härkönen and M. Bruzzi, *Concept of double peak electric field distribution in the development of radiation hard silicon detectors*, *Nucl. Instrum. Meth.* **A 583** (2007) 77.

[29] A. Junkes, *Influence of radiation induced defect clusters on silicon particle detectors*, Ph.D. Thesis, Hamburg U. (2011) [DESY-THESIS-2011-031].

[30] I. Pintilie, E. Fretwurst, G. Lindström and J. Stahl, *Close to midgap trapping level in 60Co gamma irradiated silicon detectors*, *Appl. Phys. Lett.* **81** (2002) 165.

[31] I. Pintilie, E. Fretwurst, G. Lindström and J. Stahl, *Second-order generation of point defects in gamma-irradiated float-zone silicon, an explanation for "type inversion"*, *Appl. Phys. Lett.* **82** (2003) 2169.

2020 JINST 15 P05006